Mesoscopic spatiotemporal theory for quantum-dot lasers

Edeltraud Gehrig and Ortwin Hess

Theoretical Quantum Electronics, Institute of Technical Physics, DLR, Pfaffenwaldring 38-40, D-70569 Stuttgart, Germany
(Received 3 May 2001; revised manuscript received 17 August 2001; published 5 February 2002)

We present a mesoscopic theory for the spatiotemporal carrier and light-field dynamics in quantum-dot lasers. Quantum-dot Maxwell-Bloch equations have been set up that mesoscopically describe the spatiotemporal light-field and interlevel/intralevel carrier dynamics in each quantum dot (QD) of a typical QD ensemble in quantum-dot lasers. In particular, this includes spontaneous luminescence, counterpropagation of amplified spontaneous emission, and induced recombination as well as carrier diffusion in the wetting layer (quantum-well media) of the quantum-dot laser. Intradot scattering via emission and absorption of phonons, as well as scattering with the carriers and phonons of the surrounding wetting layer are dynamically included on a mesoscopic level. The spatiotemporal light-field dynamics reveals a characteristic interplay of spontaneous and stimulated emission in quantum-dot lasers that depends on typical spatial fluctuations in size and energy levels of the quantum dots and irregularities in the spatial distribution of the quantum dots in the active layer. Those effects are simulated via statistical methods. They are shown to directly affect the propagation of an ultrashort pulse in a quantum-dot waveguide. The strong influence of the localized carrier dynamics is seen in the selective depletion and refilling of quantum-dot energy levels.

I. INTRODUCTION

The quantum-dot laser (QDL) is a complex nonlinear system in which the spatiotemporal dynamics of the propagating light fields is fundamentally linked with the physical properties of an ensemble of QDs. To unravel the complexity of this interplay a profound theoretical analysis of this novel laser type is necessary, in particular, for an interpretation of recent experimental results. Furthermore, clear insight is needed for the technological design of quantum-dot lasers with improved physical properties. The impressive technological progress in the field of quantum-dot lasers has in recent years lead to the development of various new theories that specifically focus on the physical properties of QDs and QDLs. While the investigation of the electronic and optical properties of QDs represents a formidable task all by itself, for the QDL, we have to set up a theoretical basis that combines the particular quantum optics of an ensemble of QDs with the particular material properties of QDs.

Various methods have been developed that allow a microscopic investigation of stationary material parameters in a semiconductor QD. This includes, e.g., the calculation of matrix elements and the analysis of the electronic structure of QDs [1–11]. Numerical methods that have been employed are based on Green's functions [1,2], kp theory [3,4], pseudopotential calculations [5,6], or use direct diagonalization of the respective Hamiltonian matrix [7,8]. In particular, the analysis of multiple-exciton complexes and many-body interactions has in recent years evolved to a main topic in QD theory [7–11]. On the basis of these many-body calculations spectral shifts and the appearance of multiline emission observed in experiments were explained [7].

Theoretical investigations of carrier-relaxation processes were done within the framework of perturbation theory [12], on the basis of a lattice approach [13] using precalculated matrix elements for the respective carrier-phonon interaction, or with wave functions obtained from simple QD potential shapes [14]. An alternative approach starts from the full-electron–longitudinal-optical-phonon Hamiltonian and approximates the system under the assumption that only few phonon modes couple to the carriers [15] to a form that provides a derivation of analytical solutions for the eigenstates and for the various relaxation mechanisms. This has allowed the investigation of excitons [14], electron-hole correlations [16], carrier-phonon interactions [13,17] (e.g., phonon bottleneck [17]), and Auger processes [18]. The interactions between QDs and surrounding layers via carrier-carrier collision processes have also been the focus of several publications [19,20]. The theoretical investigation of carrier-relaxation processes provides a qualitative modeling of emission spectra [12] on the basis of analytical spectral functions. Furthermore, the influence of QD size and geometry on carrier relaxation has been analyzed [21]. However, those calculations use spatially averaged quasiequilibrium distributions for the carriers and phonons, and do not consider the interaction with a spatiotemporally varying light field. Consequently they are not appropriate for the analysis of spatial effects such as the influence of a propagating light field or spatial fluctuations on the QD parameters (size, level energies).

Dynamic theories [22–32] have been set up that apply time-dependent equations for the carrier dynamics (e.g., using a density-matrix approach [22], the Green's formalism [23,24], or rate equations for the averaged carrier distributions in the QD [25–28]). The numerical modeling of the carrier dynamics has been used to calculate spontaneous-emission spectra of QDLs [26] and to discuss the various relaxation and recombination processes [27]. However, since they refer to the quasistationary situation or to the "slow" dynamics of QDL, where fast-energy relaxation or interlevel scattering are neglected or only considered via a phenomenological rate, they are only valid when the carrier distributions are near their stationary equilibrium. As an alternative approach theories on the basis of master equations [29,30] were
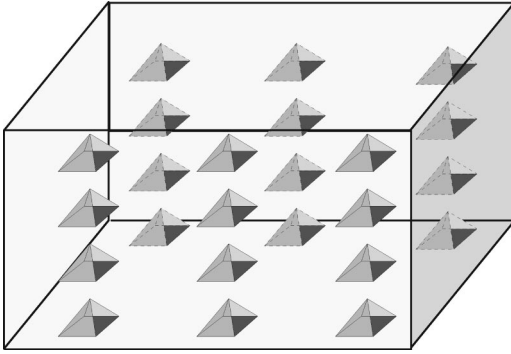
FIG. 1. Schematic of an idealized active layer of a quantum-dot laser: Columns of idential pyramidal quantum dots are aligned on a perfect grid.

FIG. 2. Representation of the quantum-dot laser model geometry. The counterpropagating light fields ($E^{\pm}$) spatiotemporally couple with carriers in the ensemble of quantum dot (columns). Characteristic fluctuations in size and location of the quantum dots are effectively represented on a numerical grid with equally spaced grid points in lateral (x) and propagation (z) directions (for details see text).

developed in which the QD ensemble is constituted of microstates, i.e., of subsystems with identical electron-hole densities. This description does not rely on the averaging of the carrier distributions. The spatial dependence of the QDs (that are embedded in the surrounding medium) and the microscopic physical properties of the individual QDs, however, have still been disregarded.

In comparison to the isolated QDs, the very particular features of a QDL—the interaction of the QDs with a spatially varying light field—have so far only been addressed in a few recent works [22,31,32]. However, due to the inherent complexity of the spatially and spectrally varying physical interactions many important characteristic properties of a QDL have so far been neglected. In particular, the spatially dependent light-field propagation and the interplay of stimulated and spontaneous emission linked with quantum fluctuations are to be combined with the individual properties of each QD (e.g., spatially varying energy levels, size, scattering processes, etc.).

In this paper we present a mesoscopic theory that bridges theoretical descriptions of microscopic material properties of QDs with macroscopic phenomenological laser theories. By explicit consideration of the complexity of the above-mentioned properties in the context of the whole laser system we introduce a realistic description of QD lasers and amplifiers. In Sec. II we derive and explain our theory, which is based on spatially resolved Maxwell-Bloch equations for QDs. Sec. III shows results of our numerical modeling, Sec. IV concludes the article.

II. THEORETICAL DESCRIPTION: QUANTUM DOT MAXWELL-BLOCH EQUATIONS

In this section, we will derive the quantum-dot Maxwell-Bloch equations (QD-MBEs). The QD-MBEs consist of semiconductor Bloch equations for an ensemble of QDs (QD-SBEs). Thereby we will, in particular, include various carrier relaxation processes (Sec. II B). To represent the dynamic subwavelength variations in the light-field dynamics we will derive from Maxwell's equations a wave equation tailored for quantum-dot lasers. The coupled system of partial differential equations then constitutes the quantum-dot Maxwell-Bloch equations that model on a mesoscopic basis
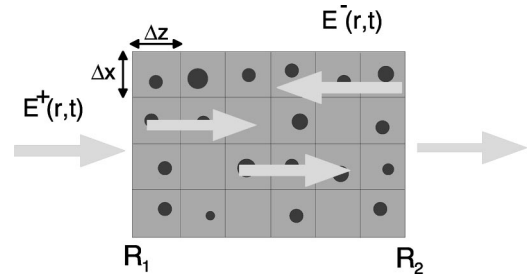
the dynamic light-matter interactions occurring within a QD laser.

Figure 1 schematically shows the typical geometry of a QDL. The active layer contains an ensemble of spatially distributed QDs that are embedded within the quantum-well wetting layer (WL). Depending on the epitaxial growth process the laser may consist of several layers defining vertical "QD stacks" (columns). Light propagates within the active layer in the resonator predominately along the longitudinal (z) direction. This dynamics of the light fields is described by Maxwell's wave equations considering the spatiotemporal changes of the light fields propagating in the forward ($+$) and backward ($-$) direction within the laser (see Fig. 2). The layered vertical (y) structure is considered via effective material and device parameters. These are, in particular, the effective refractive index and the guiding properties of the layer as well as the physical properties of the QD stack (vertically averaged energy levels, damping rates or QD size). The vertically averaged physical properties characterize an "effective" QD. The properties that enter the QD-SBEs in a self-consistent way are, in particular, the energy levels, the initial occupation of the levels (established, e.g., via optical or electrical pumping), and the size of the QDs.

Via the polarization of the active QD medium, the light fields are locally coupled to the dynamics of the carriers and to the interlevel dipole dynamics (described on the basis of the QD-SBEs). Thereby the individual time scales of the underlying optical and electronic processes spanning a temporal regime from femtoseconds up to nanoseconds are mesoscopically represented. In particular, their spatial and spectral characteristics are fully taken into account and include, e.g., the localization of the dots in the medium, fluctuations in size and shape of the QDs, the spatially dependent light-field propagation, and diffraction as well as spatially dependent scattering processes and carrier transport.

The time-dependent calculation of the carrier distributions and light-field dynamics allow for an explicit consideration of the individual time scales of the various interaction processes. The relevant time scales range from the femtosecond regime (for the fast carrier-scattering processes) up to the picosecond and nanosecond regimes (for the dynamics of the propagating light fields and of the spatial carrier density).

A. Carrier dynamics within a QD

Starting from the single-particle density matrices for the electrons, $n^e = \langle c^\dagger c \rangle$, and holes, $n^h = \langle d^\dagger d \rangle$, and for the interlevel polarization, $p = \langle d^\dagger c \rangle$, where c and d are the local annihilation operators for electrons and holes, respectively, one can derive semiconductor Bloch equations specifically for quantum dots. The resulting QD-SBEs mesoscopically describe the dynamic changes of the electron and hole distributions inside the dot (for each energy level) and the dynamics of the (interlevel) dipoles. If one considers an ensemble of quantum dots as active medium in a quantum-dot laser, additional terms and effects are of relevance. These are contributions describing the electrical injection of carriers (pumping) Λ^e (including Pauli blocking), induced recombination (with generation rate $g^{e,h}$), spontaneous recombination of the carriers (Γ_{sp}), carrier-carrier and carrier-phonon scattering for the intradot relaxation ($\partial n^{e,h}/\partial t|_{QD}^{c\text{-}ph}$), and the interaction with the wetting layer ($\partial n^{e,h}/\partial t|_{QD\text{-}WL}$). The dynamics of the occupation of electrons (e, level index i) and holes (h, level index j) , $n^{e,h}$, and the dynamics of the interlevel polarizations $p^\pm$ [coupled to the forward $(+)$ and backward $(-)$ propagating optical fields] within a QD are then governed by the equations of motion

$$\frac{\partial n^e(i)}{\partial t} = \Lambda^e(i)[D^e(i) - n^e(i)] + g^e(i) - \gamma^{nr} n^e(i)$$

$$- \sum_j \Gamma_{sp} n^e(i) n^h(j)$$

$$+ \left.\frac{\partial n^e(i)}{\partial t}\right|_{QD}^{c\text{-}ph} + \left.\frac{\partial n^e(i)}{\partial t}\right|_{QD\text{-}WL},$$

$$\frac{\partial n^h(j)}{\partial t} = \Lambda^h(j)[D^h(j) - n^h(j)] + g^h(j) - \gamma^{nr} n^e(i)$$

$$- \sum_i \Gamma_{sp} n^h(j) n^e(i)$$

$$+ \left.\frac{\partial n^e(i)}{\partial t}\right|_{QD}^{c\text{-}ph} + \left.\frac{\partial n^e(i)}{\partial t}\right|_{QD\text{-}WL},$$

$$\frac{\partial p^\pm(j,i)}{\partial t} = -(i\bar\omega(j,i) + \gamma_p) p^\pm(j,i) - \frac{i}{\hbar}[n^e(i) + n^h(j)]\mathcal{U}^\pm$$

$$- \frac{i}{\hbar}\delta\mathcal{U}_{nl}^\pm + F_p q^p + \left.\frac{\partial p^\pm(j,i)}{\partial t}\right|_{QD}^{p\text{-}ph}, \qquad (1)$$

where γ_{nr} represents the rate due to nonradiative recombination and τ_p denotes the dephasing time of the interlevel dipole. The pump term

$$\Lambda^c(l) = \Gamma_{QD} \frac{I\eta}{eh} \frac{n_{eq}^c(l)}{\sum_l n_{eq}^c(l)[D^{e,h}(l) - n^c(l)]} \qquad (2)$$

mesoscopically represents the carrier injection and includes the pump-blocking effect ($c = e,h$ and $l = i,j$ for electrons and holes, respectively). It depends on the absolute injection current I, pump efficiency η, and the thickness of the active area, h. $D^c(l)$ denotes the degeneracy of an end energy level (i.e., the maximum occupation with carriers). Γ_{QD} describes the reduction of the pump efficiency resulting from the vertically arranged QDs, i.e., the "spatial overlap" between carrier injection and a vertical stack of QDs in the medium.

The generation rates given by

$$g^e(i) = \text{Re}\left[\frac{i}{\hbar} \sum_j [\{\mathcal{U}^+ p_{nl}^{+*}(j,i) + \mathcal{U}^- p_{nl}^{-*}(j,i)\}\right.$$

$$\left. - \{\mathcal{U}^{+*} p_{nl}^+(j,i) + \mathcal{U}^{-*} p_{nl}^-(j,i)\}]\right],$$

$$g^h(j) = \text{Re}\left[\frac{i}{\hbar} \sum_i [\{\mathcal{U}^+ p_{nl}^{+*}(j,i) + \mathcal{U}^- p_{nl}^{-*}(j,i)\}\right.$$

$$\left. - \{\mathcal{U}^{+*} p_{nl}^+(j,i) + \mathcal{U}^{-*} p_{nl}^-(j,i)\}]\right] \qquad (3)$$

depend on the interlevel polarization p and on the optical field contributions of spontaneous and induced emission constituting the local field $\mathcal{U}^\pm$. The Langevin noise term $F_p q^p$ describes dipole fluctuations [33] with amplitude $F_p = \Gamma \sqrt{2\hbar\epsilon_r}/n_l^2 L \sqrt{\epsilon_0 \omega_0}$. The local fields $\mathcal{U}^\pm = d(j,i)E^\pm + \delta\mathcal{U}^\pm$ are composed of the optical light-field contributions $E^\pm$ as well as those induced by Coulomb screening within each quantum dot and by the Coulomb interactions between the carriers in the QD and the carriers in the wetting layer, $\delta\mathcal{U}$. $d(j,i)$ is the interlevel dipole matrix element. The interlevel polarization depends via $\bar\omega(j,i) = \hbar^{-1}(\mathcal{E}^e + \mathcal{E}^h) - \omega$ (ω is the frequency of the propagating light fields) on the carrier energies $\mathcal{E}^{e,h}$ that are given by

$$\mathcal{E}^c(l) = \epsilon^c(l) + \delta\mathcal{E}^c(l), \qquad (4)$$

with the unperturbed level energies $\epsilon^{e,h}$ (i.e., neglecting the carrier dynamics). The characteristic level energies $\epsilon^c(l)$ of the unperturbed QD are taken from microscopic material calculations [3] and are self-consistently included in the theory. The Coulomb-induced screening that leads to a renormalization of these energy levels and also results in additional local-field contributions strongly depends on the specific QD design (size, shape). These respective corrections have been determined in detailed calculations (e.g., [16,21,34]) and are represented in the QD-SBEs [Eq. (1)] in the form of spatially dependent energies ($\hbar\bar\omega$ and local-field contributions $\delta\mathcal{U}^\pm$).

B. Carrier relaxation dynamics

Within each quantum dot the relaxation of the electrons and holes is determined by a variety of physical mechanisms. These are the intradot relaxation $[\partial n^c(l)/\partial t|_{QD}]$ via acoustical and optical phonons or multiphonon processes and scattering $[\partial n^{e,h}(i)/\partial t|_{QD\text{-}WL}]$ between the carriers in the QD and the carriers and phonons of the wetting layer. The physi-

cal properties of an individual QD (size, shape, energy levels) and the phonon distribution thereby determine the relevance of the various relaxation processes. Here we will use dynamic scattering rates for carrier-phonon-relaxation processes on the basis of microscopically determined matrix elements for the respective interaction. The elastic scattering between the QD carriers and the carriers of the wetting layer will be considered on the basis of perturbation theory.

1. Intradot relaxation

The scattering rates for carrier-phonon intradot relaxation generally include emission $(-)$ and absorption $(+)$ of longitudinal acoustical (LA) phonons, longitudinal optical (LO) phonons, and, in particular, multiphonon processes $(\pm 2 \text{ LO}, \pm 2 \text{ LA, and } \pm\text{LO}\pm\text{LA})$. They are determined on the basis of microscopic calculations allowing, via a dependence of the rates on the spatially and temporally varying carrier and phonon distributions within the QD and the surrounding layers, a self-consistent mesoscopic inclusion of all scattering processes that are relevant in QD lasers. The quantum kinetic equations of motion of the single-particle density matrices with respect to the carrier-phonon Hamiltonian are given by

$$\frac{\partial n^e}{\partial t}\bigg|_{QD}^{e\text{-}ph}(i)=2\sum_{\mathbf{q}}\sum_{i_1,i_2}\{\text{Re}[s_q^e(i_1,i)]-\text{Re}[s_q^e(i,i_2)]\},$$

$$\frac{\partial n^h}{\partial t}\bigg|_{QD}^{h\text{-}ph}(j)=2\sum_{\mathbf{q}}\sum_{j_1,j_2}\{\text{Re}[s_q^h(j_1,j)]-\text{Re}[s_q^h(j,j_2)]\},$$

$$\frac{\partial p}{\partial t}\bigg|_{QD}^{p\text{-}ph}(j,i)=\sum_{\mathbf{q}}\bigg[\sum_{j_1}[t^{(+)}(j_1,i)-t^{(-)*}(j_1,i)]$$
$$-\sum_{i_1}[t^{(+)}(j,i_1)-t^{(-)*}(j,i_1)]\bigg], \quad (5)$$

where i and j are the initial (in the case of phonon emission) or final (in the case of phonon absorption) level of the electrons (i) and holes (j) and i_1, i_2, j_1, j_2 denote intermediate levels from which inscattering and outscattering occurs via the emission and absorption of phonons. The intraband density matrices

$$s_q^e(i_1,i_2)=\frac{i}{\hbar}\langle g_{\mathbf{q}}^e c_{i_1}^\dagger b_{\mathbf{q}} c_{i_2}\rangle,$$

$$s_q^h(j_1,j_2)=\frac{i}{\hbar}\langle g_{\mathbf{q}}^h d_{j_1}^\dagger b_{\mathbf{q}} d_{j_2}\rangle \quad (6)$$

depend on the carrier (c_i,d_j) and phonon ($b_{\mathbf{q}}$) creation and annihilation operators ($\mathbf{q}$ denotes the phonon wave vector). They describe energy relaxation. $g_{\mathbf{q}}^{e,h}$ is the coupling constant of the respective carrier-phonon interaction [35]. The interlevel density matrices

$$t_q^{(+)}(j,i)=\frac{i}{\hbar}\langle g_{\mathbf{q}}^p d_j b_{\mathbf{q}} c_i\rangle,$$

$$t_q^{(-)*}(j,i)=\frac{i}{\hbar}\langle g_{\mathbf{q}}^p d_j b_{\mathbf{q}}^\dagger c_i\rangle \quad (7)$$

describe phase-relaxation processes.

We start from the Heisenberg picture to derive a quantum kinetic equation of motion for the phonon-assisted density matrices. To include the emission and absorption of phonons, contributions up to second order have to be considered. Factorization of the two-particle matrices into two single-particle density matrices, e.g., $\langle c^\dagger c^\dagger b_{\mathbf{q}'}^\dagger b_{\mathbf{q}}\rangle = n^e n_{\mathbf{q}} \delta_{\mathbf{q},\mathbf{q}'}$, and using the Markov approximation (i.e., assuming slowly varying distributions) leads to a semiclassical description where only the expectation values of the electrons, holes, and of the interlevel polarization appear and cross-correlation effects are neglected. The reduced equations of motion then read

$$\frac{\partial s^e(i_1,i_2)}{\partial t}=-\left(\frac{i}{\hbar}(\mathcal{E}_{i_1}-\mathcal{E}_{i_2}-\mathcal{E}_{ph})+\gamma_{\mathbf{q}}^e\right)s^e(i_1,i_2)$$
$$+\frac{1}{\hbar^2}|g_{\mathbf{q}}^e|^2\{(n_{\mathbf{q}}+1)n^e(i_1)[D^e(i_2)-n^e(i_2)]$$
$$-n_{\mathbf{q}}n^e(i_2)[D^e(i_1)-n^e(i_1)]\}$$
$$-\sum_j\left(\frac{i}{\hbar}\mu(j,i_1)+\gamma_{\mathbf{q}}^h\right)^*t^{(+)}(j,i_2)$$
$$-\sum_j\left(\frac{i}{\hbar}\mu(j,i_2)+\gamma_{\mathbf{q}}^h\right)t^{(-)}(j,i_1)$$
$$-\sum_j\frac{1}{\hbar^2}g_{\mathbf{q}}^e g_{\mathbf{q}}^{h*}p^*(j,i_1)p(j,i_2),$$

$$\frac{\partial s^h(j_1,j_2)}{\partial t}=-\left(\frac{i}{\hbar}(\mathcal{E}_{j_1}-\mathcal{E}_{j_2}-\mathcal{E}_{ph})+\gamma_{\mathbf{q}}^h\right)s^h(j_1,j_2)$$
$$+\frac{1}{\hbar^2}|g_{\mathbf{q}}^h|^2\{(n_{\mathbf{q}}+1)n^h(j_1)[D^h(j_2)-n^h(j_2)]$$
$$-n_{\mathbf{q}}n^h(j_2)[D^h(j_1)-n^h(j_1)]\}$$
$$-\sum_i\left(\frac{i}{\hbar}\mu(j_1,i)+\gamma_{\mathbf{q}}^e\right)^*t^{(+)}(j_2,i)$$
$$-\sum_i\left(\frac{i}{\hbar}\mu(j_2,i)+\gamma_{\mathbf{q}}^e\right)t^{(-)}(j_1,i)$$
$$-\sum_j\frac{1}{\hbar^2}g_{\mathbf{q}}^h g_{\mathbf{q}}^{e*}p^*(j_1,i)p(j_2,i),$$

$$\frac{\partial t^{(+)}(j,i)}{\partial t}=-\left(\frac{i}{\hbar}(\mathcal{E}_j+\mathcal{E}_i-\mathcal{E}_{ph})+\gamma_{\mathbf{q}}^p\right)t^{(+)}(j,i)$$
$$-\sum_j\frac{1}{\hbar^2}|g_{\mathbf{q}}^p|^2\{n_{\mathbf{q}}n^h(j)+(n_{\mathbf{q}}+1)[D^h(j)$$
$$-n^h(j)]\}p(j,i)-\sum_i\frac{1}{\hbar^2}|g_{\mathbf{q}}^p|^2\{n_{\mathbf{q}}n^e(i)$$

$$+ (n_{\mathbf{q}}+1)[D^e(i)-n^e(i)]\}p(j,i)$$

$$+ \sum_{i_1} \left(\frac{i}{\hbar}\mu(j,i_1)+\gamma_{\mathbf{q}}^e \right)^{*} s^e(i_1,i)$$

$$- \sum_{j_1} \left(\frac{i}{\hbar}\mu(j_1,i)+\gamma_{\mathbf{q}}^h \right) s^h(j_1,j), \qquad (8)$$

where the damping arising from higher-order terms are included in $\gamma_{\mathbf{q}}^c = \gamma_{\mathbf{q}}^c(l_1)+\gamma_{\mathbf{q}}^c(l_2)$ and $\gamma_{\mathbf{q}}^p$.

Typical time scales of the phonon dynamics are slow in comparison with the carrier dynamics. Moreover, due to the conservation of energy, only phonons with energies close to resonance with the level energies of the QDs significantly contribute to the carrier-phonon interactions. Thus one can adiabatically eliminate the dynamics of the density matrices. Furthermore, the phonon distributions are approximated with their quasiequilibrium distribution given by the respective Bose statistics, $n_q = 1/[\exp(\hbar\omega_q/kT)-1]$ with phonon frequency $\omega_{\mathbf{q}}$. Insertion of the resulting expression for the matrices $s^{e,h}$, $t^{(\pm)}$ yields the following rates describing the change in level occupation by inscattering and outscattering processes:

$$\left.\frac{\partial n^e(i)}{\partial t}\right|_{QD}^{e\text{-}ph} = \sum_{i_1>i} 2\frac{|g^e|^2}{\hbar}\mathcal{L}^e(i_1,i)\{(n_q+1)n^e(i_1)[D^e(i)-n^e(i)]-n_q n^e(i)[D^e(i_1)-n^e(i_1)]\}$$

$$- \sum_{i_1<i} 2\frac{|g^e|^2}{\hbar}\mathcal{L}(i,i_1)\{(n_q+1)n^e(i)[D^e(i_1)-n^e(i_1)]-n_q n^e(i1)[D^e(i)-n^e(i)]\}$$

$$- \sum_j \left[\sum_{j_1<j} \left\{ 2\frac{g^h g^{e*}}{\hbar}\mathcal{L}(j,j_1)p(i,j_1)p^*(i,j)-2\frac{g^{h*}g^e}{\hbar}\mathcal{L}(j,j_1)p^*(i,j_1)p(i,j) \right\} \right.$$

$$\left. - \sum_{j_1>j} \left\{ 2\frac{g^h g^{e*}}{\hbar}\mathcal{L}(j_1,j)p(i,j_1)p^*(i,j)-2\frac{g^{h*}g^e}{\hbar}\mathcal{L}(j_1,j)p^*(i,j_1)p(i,j) \right\} \right],$$

$$\left.\frac{\partial n^h(j)}{\partial t}\right|_{QD}^{h\text{-}ph} = \sum_{j_1>j} 2\frac{|g^h|^2}{\hbar^2}\mathcal{L}^h(j_1,j)\{(n_q+1)n^h(j_1)[D^h(j)-n^h(j)]-n_q n^h(j)[D^h(j_1)-n^h(j_1)]\}$$

$$- \sum_{j_1<j} 2\frac{|g^h|^2}{\hbar^2}\mathcal{L}^h(j,j_1)\{(n_q+1)n^h(j)[D^h(j_1)-n^h(j_1)]-n_q n^h(j_1)[D^h(j)-n^h(j)]\}$$

$$- \sum_i \left[\sum_{i_1<i} \left\{ 2\frac{g^e g^{h*}}{\hbar}\mathcal{L}(i,i_1)p(i_1,j)p^*(i,j)-2\frac{g^{e*}g^h}{\hbar}\mathcal{L}(i,i_1)p^*(i_1,j)p(i,j) \right\} \right.$$

$$\left. - \sum_{i1>i} \left\{ 2\frac{g^e g^{h*}}{\hbar}\mathcal{L}(i_1,i)p(i_1,j)p^*(i,j)-2\frac{g^{e*}g^h}{\hbar}\mathcal{L}(i_1,i)p^*(i_1,j)p(i,j) \right\} \right]. \qquad (9)$$

The function $\mathcal{L}$ describes the dependence of the carrier-phonon interaction on the contributing QD level energies and the energy of the respective phonon. It also contains the damping resulting from higher-order contributions. For carriers interacting with an optical (LO) phonon, $\mathcal{L}$ can be expressed with a Lorentzian line shape

$$\mathcal{L}(l_1,l_2) = \frac{\tau_{LO}^{-1}}{\hbar^{-2}(\mathcal{E}_{l_1}-\mathcal{E}_{l_2}-\mathcal{E}_{LO})^2+\tau_{LO}^{-2}} \qquad (10)$$

with $l=i$ for electrons and $l=j$ for holes. The lifetime τ_{LO} with

$$\tau_{LO}^{-1} = \frac{2\pi}{\hbar^2}|V^{Anh}|^2\sum_q \delta(2\omega_{LA}(q)-\omega_{LO})[2n_q+1] \qquad (11)$$

includes the decay of optical phonons into two acoustical phonons via the inharmonic interaction potential V^{Anh}. The lifetime of acoustical phonons usually is much longer than the lifetime of optical phonons. As a result, the function $\mathcal{L}$ can in the case of direct interaction of carriers with acoustical phonons be approximated with a δ function, $\mathcal{L}^c(l_1,l_2) = \delta(\mathcal{E}_{l_1}-\mathcal{E}_{l_2}-\mathcal{E}_{ph})$.

Next to the emission and absorption of one single phonon the influence of multiphonon relaxation has to be considered. Among all multiphonon processes the most relevant ones are the emission/absorption of an LO phonon accompanied with the absorption/emission of an acoustical phonon ($\pm$LO $\pm$LA) and the emission/absorption of two acoustical phonons ($\pm$LA$\pm$LA). The respective relaxation terms derived in analogy to the above read

$$\frac{\partial n^c}{\partial t}\bigg|_{c\text{-}2ph}(l)=2\sum_{l_1>l}\sum_{l_1>l>l_2}\frac{1}{\hbar}|g_1^c(q_1)g_2^c(q_2)\mathcal{L}_{q_1}(l_1,l_2)+g^e(q_1)g^e(q_2)\mathcal{L}_{q_2}(l,l_2)|^2\{(n_{q_2}n_{q_1}+1)n^c(l_1)[D^c(l)-n^c(l)]$$

$$-(n_{q_2}+1)n_{q_1}n^c(i)[D^c(l_1)-n^c(l_1)]\}+2\sum_{l_1>l}\sum_{l_1>l_2>l}\frac{1}{\hbar}|g_1^c(q_1)g_2^c(q_2)\mathcal{L}_{q_1}(l_2,l)+g_1^c(q_1)g_2^c(q_2)\mathcal{L}_{q_2}(l_1,l_2)|^2$$

$$\times\{(n_{q_2}+1)(n_{q_1}+1)n^c(l_1)[D^c(l)-n^c(l)]-n_{q_2}n_{q_1}n^c(i)[D^c(l_1)-n^c(l_1)]\}+2\sum_{l_1>l}\sum_{l_2>l_1>l}\frac{1}{\hbar}$$

$$\times|g_1^c(q_1)g_2^c(q_2)\mathcal{L}_{q_1}(l_2,l)+g_1^c(q_1)g_2^c(q_2)\mathcal{L}_{q_2}(l_2,l_1)|^2\{n_{q_2}(n_{q_1}+1)n^c(l_1)[D^c(l)-n^c(l)]$$

$$-(n_{q_2}+1)n_{q_1}n^c(i)[D^c(l_1)-n^c(l_1)]\}+2\sum_{l>l_1}\sum_{l>l_1>l_2}\frac{1}{\hbar}|g_1^c(q_1)g_2^c(q_2)\mathcal{L}_{q_1}(l,l_2)+g^e(q_1)g^e(q_2)\mathcal{L}_{q_2}(l_1,l_2)|^2$$

$$\times\{(n_{q_2}+1)n_{q_1}n^c(l_1)[D^c(l)-n^c(l)]-(n_{q_2}+1)n_{q_1}n^c(i)[D^c(l_1)-n^c(l_1)]\}+2\sum_{l>l_1}\sum_{l>l_2>l_1}\frac{1}{\hbar}$$

$$\times|g_1^c(q_1)g_2^c(q_2)\mathcal{L}_{q_1}(l,l_2)+g_1^c(q_1)g_2^c(q_2)\mathcal{L}_{q_2}(l_2,l_1)|^2\{n_{q_2}n_{q_1}n^c(l_1)[D^c(l)-n^c(l)]$$

$$-(n_{q_2}+1)(n_{q_1}+1)n^c(i)[D^c(l_1)-n^c(l_1)]\}+2\sum_{l_1>l}\sum_{l_2>l>l_1}\frac{1}{\hbar}$$

$$\times|g_1^c(q_1)g_2^c(q_2)\mathcal{L}_{q_1}(l_2,l_1)+g_1^c(q_1)g_2^c(q_2)\mathcal{L}_{q_2}(l_2,l)|^2\{(n_{q_2}+1)n_{q_1}n^c(l_1)[D^c(l)-n^c(l)]$$

$$-n_{q_2}(n_{q_1}+1)n^c(i)[D^c(l_1)-n^c(l_1)]\}, \tag{12}$$

where $\mathcal{L}_{q_1}$, $\mathcal{L}_{q_1}$ depend on the energy and damping rate of the respective phonon.

2. Scattering processes between QDs and the wetting layer

Next to the intradot relaxation, the dynamics of the quantum-dot laser depends on the carrier-carrier and carrier-phonon scattering processes that occur between the QDs and the wetting layer into which they are embedded. Those are both, inelastic emission and absorption of phonons as well as elastic collision processes. For the inelastic-scattering processes we will consider the inelastic Coulomb interaction between QD carriers and the 2D carrier plasma of the wetting layer via Auger recombination, the ionization of a QD via excitation of carriers by absorption of a phonon, as well as the carrier capture from the wetting layer in a (up to then unoccupied) state of the QD by emission of a phonon, i.e.,

$$\frac{\partial n^c(l)}{\partial t}\bigg|_{QD\text{-}WL}=\frac{\partial n^c(l)}{\partial t}\bigg|_{QD\text{-}WL}^{Aug}+\frac{\partial n^c(l)}{\partial t}\bigg|_{QD\text{-}WL}^{c\text{-}ph}. \tag{13}$$

The relaxation rates

$$\frac{\partial n^c}{\partial t}\bigg|_{QD\text{-}WL}^{c\text{-}ph}(l)=\{f_{QD\text{-}WL}^e N_{WL}^c[D^c(l)-n^c(l))(n_{\mathbf{q}}+1]$$

$$-n^c n_{\mathbf{q}}(\Delta\mathcal{E}(l))\}\mathcal{L}(l,\infty) \tag{14}$$

describe the interactions between the discrete energy levels of the QDs and the states of the surrounding quantum-well

layer via emission and absorption of optical and acoustical phonons, where the level description ∞ in $\mathcal{L}(l,\infty)$ refers to the respective energy of the valence and conduction bands of the wetting layer. In Eq. (14) the scaling factor $f_{QD\text{-}WL}^e$ represents the fraction of wetting layer states to which a single (effective) QD couples. It is determined by the dot density and by the epitaxial structure defining, e.g., the potential barrier between the QD and the surrounding layers. $n_q(\Delta\mathcal{E}(l))$ denotes the phonon number available at energy values higher than the energy given by the potential step between the respective QD level and the wetting layer. The Auger carrier-capture kinetics may be attributed to the following processes.

(1) A QD electron or hole in the wetting layer collides with a 2D electron and is captured by the QD. The final state of the second 2D electron is then a wetting-layer state of higher energy.

(2) A 2D hole is captured via Coulomb scattering with a QD electron into the dot while the electron is excited into a wetting-layer state.

We will represent the two types of processes with the rates [36]

$$\frac{\partial n^e}{\partial t}\bigg|_{QD\text{-}WL}^{Aug}(i)=-\sum_j B_{he}N_{WL}^h n^e(i)[D^h(j)-n^h(j)]$$

$$+C_{ee}N_{WL}^{e2}[D^e(i)-n^e(i)]$$

$$+C_{eh}N_{WL}^e N_{WL}^h[D^e(i)-n^e(i)],$$

$$\frac{\partial n^e}{\partial t}\bigg|_{QD\text{-}WL}^{Aug}(j) = B_{he}N_{wl}^h\sum_i n^e(i)[D^h(j)-n^h(j)]$$

$$+ C_{hh}N_{WL}^h{}^2[D^h(j)-n^h(j)]$$

$$+ C_{he}N_{WL}^h N_{WL}^e[D^h(j)-n^h(j)]. \quad (15)$$

In the wetting layer, the carriers are not as strongly localized as in the quantum-dot islands and may therefore diffuse within the layer. With $N_{WL}^{e,h}$ denoting the local density of electrons ($c=e$) and holes ($c=h$), the dynamics of wetting-layer carriers is represented by the diffusion equation

$$\frac{\partial N_{WL}^c}{\partial t} = \frac{J}{ed} + \frac{\partial N^c}{\partial t}\bigg|_{QD\text{-}WL} - \gamma_{sp}N^e{}_{WL}N_{WL}^h - \gamma_{WL}^{nr}N_{WL}^c, \quad (16)$$

with a pump term describing carrier injection and a rate for nonradiative emission processes. In Eq. (16) the change in carrier density due to Auger relaxation can be expressed as [36]

$$\frac{\partial N^e}{\partial t}\bigg|_{QD\text{-}WL} = B_{he}N_{WL}^h n^e(i)[D^h(j)-n^h(j)]n_{QD}$$

$$- C_{ee}N_{WL}^e{}^2[D^e(i)-n^e(i)]n_{QD}$$

$$- C_{eh}N_{WL}^e N_{WL}^h[D^e(i)-n^e(i)]n_{QD},$$

$$\frac{\partial N^e}{\partial t}\bigg|_{QD\text{-}WL} = - B_{he}N_{WL}^h f^e(i)[D^h(j)-n^h(j)]n_{QD}$$

$$- C_{hh}N_{WL}^h{}^2[D^h(i)-n^h(i)]n_{QD}$$

$$- C_{he}N_{WL}^h N_{WL}^e[D^h(j)-n^h(i)]n_{QD}. \quad (17)$$

In Eq. (15) and (17) B_{he}, C_{ee}, C_{eh}, and C_{he} are the respective Auger capture coefficients, which we take from the detailed calculation in [36], n_{QD} is the dot density.

The elastic Coulomb-scattering processes between the QDs and the wetting layer are treated on the basis of perturbation theory [19,20]. Elastic collisions do not change the occupation of the levels. However, they may lead to significant changes in electronic energies and damping that result in a spectral shift and spectral broadening represented by an energy-correction term $\delta\mathcal{E}^{e,h}$ and the dipole damping τ_p. These spatiotemporally varying quantities are self-consistently included in the QD-SBEs. They lead to spatially dependent line shapes and frequency differences $\bar{\omega}$ between the frequency of the propagating light field and the eigenfrequencies of the spatially localized QDs in the laser structure. The shift of the emission frequency and the carrier damping rate resulting from the elastic Coulomb scattering between QD and the surrounding layer are

$$\Delta\omega_{QD\text{-}WL}^{e,h} = \sqrt{2kT/m^{e,h}}\,\sigma_\omega N_{WL}^{e,h},$$

$$\Delta\gamma_{QD\text{-}WL}^{e,h} = \sqrt{2kT/m^{e,h}}\,\sigma_\gamma N_{WL}^{e,h}, \quad (18)$$

where $\sigma_\gamma^{e,h}$ and $\sigma_\omega^{e,h}$ denote the intersection areas of the scattering processes given by [20]

$$\sigma_\gamma^{e,h} = \int_0^\infty 2db_{QD}\left[1 - \cos\left(\int_{-\infty}^\infty dt\Delta\omega_{QD}^{e,h}(t)\right)\right],$$

$$\sigma_\omega^{e,h} = \int_0^\infty 2db_{QD}\sin\left(\int_{-\infty}^\infty dt\Delta\omega_{QD}^{e,h}(t)\right), \quad (19)$$

with

$$\Delta\omega_{QD}^{e,h} = -\frac{C_3^{e,h}}{r_{QD}^3} - \frac{C_4^{e,h}}{r_{QD}^4},$$

$$C_3^{e,h} = \frac{\pm e^2}{4\pi\varepsilon_0 n_{eff}^2\hbar}\frac{\beta h_{QD}^2}{2},$$

$$C_4^{e,h} = \frac{e^2}{16\pi^2\varepsilon_0^2 n_{eff}^4\hbar}\frac{k_F}{\hbar}. \quad (20)$$

The sign $\pm$ in $C_3^{e,h}$ refers to the situation where the carriers in the QD and in the wetting layers that participate in the collision process have equal ($+$) or different ($-$) signs, respectively. b_{QD} is the spatially dependent collision parameter, h_{QD} and r_{QD} are the height and the radius of the QD. n_{eff} is the effective index of the material. The coefficient β is a measure of the linear Stark effect (resulting from expressing the component of the dipole in direction of the QD axis as βh_{QD}) and k_F is a coefficient describing the quadratic Stark effect, which can be estimated from the dipole moment and the eigenenergies [37]. The collision-induced correction $\Delta\omega_{QD\text{-}WL}^{e,h}$ is added to the spatially dependent energy renormalization $\delta\mathcal{E}$ and $\Delta\gamma_{QD\text{-}WL}^{e,h}$ contributes to the damping rates $\gamma^{e,h}$ and γ^p in the density matrices. We note that the spatial dependence of b_{QD}, r_{QD}, and h_{QD} modeled in the form ($p=b_{QD},h_{QD},r_{QD}$)

$$p_{QD} = p_{QD}^{av}(1 + p_{QD}^{fluc}), \quad (21)$$

where p_{QD}^{av} denotes the average value and p_{QD}^{fluc} is the spatially dependent fluctuation, represents an arbitrarily distributed ensemble of quantum dots of varying size and shape. b_{QD}^{fluc} considers, for example, the spatial fluctuation of the collision parameter resulting from a spatial localization of the QDs in the laser. The higher the amplitude of the fluctuations, the higher is the degree of disorder in the spatial distribution of the effective QDs. r_{QD} and h_{QD} are the average radius and height of the QDs, respectively. This leads to spatially dependent energy corrections and damping rates.

The QD-SBEs including the dynamic intradot scattering and the interactions with the wetting layer constitute a fundamental basis for a microscopic analysis of the relevant physical processes such as the influence of many-body interactions, spontaneous recombination, carrier relaxation, and carrier injection. At each location in the laser structure the carrier dynamics within the QD (1) and the wetting layer (16) is—via the generation rate and the dipole dynamics—

fundamentally linked to the light-field dynamics that, in turn, is described by a suitable wave equation.

C. Optical field dynamics: Counterpropagation and diffraction

The spatiotemporal light-field dynamics plays a major role for relevant physical quantities such as the spatiospectral gain and induced index of the system that, in combination with the complex carrier dynamics, determine output quantities of the laser system, i.e., emission wavelength, spectral bandwidth, saturation properties, and temporal emission characteristics. A realistic theoretical treatment consequently requires full consideration of spatially and temporally varying optical fields (associated with spontaneous- and induced-emission processes) that are mesoscopically coupled to the dynamics of the electrons and holes in the QDs. The QD ensemble represents a strongly inhomogeneous gain medium with spatially distributed QDs with individual material properties (dielectric constant, refractive index, etc.). This spatial inhomogeneity is even more intensified by the spatiotemporal dynamics of the carrier distributions in the QDs and in the wetting layer as well as by the nonlinear interaction of both carrier systems with each other. One may immediately sense that these space- and time-dependent variations lead to strong phase changes during the propagation of the light fields in the laser resonator. Consequently the calculation of the light-field dynamics has to include the temporal and spatial changes of the field amplitudes in an appropriate manner.

We start from Maxwell's equations for the optical field **E** and the polarization **P** and the material equations and derive the wave equation

$$\frac{1}{\varepsilon_0}\nabla\nabla\cdot\mathbf{P}+\nabla^2\mathbf{E}-\frac{1}{c^2}\frac{\partial^2}{\partial t^2}\mathbf{E}=\mu_0\frac{\partial^2}{\partial t^2}\mathbf{P}, \qquad (22)$$

where ε_0 and μ_0 are the permittivity and the permeability in vacuum, respectively, c is the velocity of light. Insertion of the ansatz

$$\mathbf{E}=e^{i\beta z-i\omega t}(E_T+e_z E_z),$$

$$\mathbf{P}=e^{i\beta z-i\omega t}(P_T+e_z P_z) \qquad (23)$$

for the optical fields and the polarization leads to

$$\left(-\beta^2+2i\beta\frac{\partial}{\partial z}+\frac{\partial^2}{\partial z^2}\right)(E_T+e_z E_z)+\nabla_T^2(E_T+e_z E_z)$$

$$-\nabla_T\nabla_T-\nabla_T E_T-\nabla_T\left(i\beta+\frac{\partial}{\partial z}\right)e_z E_z$$

$$-\left(i\beta+\frac{\partial}{\partial z}\right)\nabla_T E_T+\frac{1}{c^2}\left(\omega^2+2i\omega\frac{\partial}{\partial t}-\frac{\partial^2}{\partial t^2}\right)$$

$$\times(E_T+e_z E_z)$$

$$=-\mu_0\left(\omega^2+2i\omega\frac{\partial}{\partial t}-\frac{\partial^2}{\partial t^2}\right)(P_T+e_z P_z), \qquad (24)$$

with the propagation constant β and frequency ω. With the main field propagation parallel and antiparallel to the resonator axis we may in Eq. (24) neglect the mixed derivatives $\nabla_T\partial/\partial z$, $(\partial/\partial z)\nabla_T$. Similarly, $\nabla_T E_T\approx-i\beta E_z$ such that the deviates $\nabla_T\nabla_T E$ and $\nabla_T i\beta E_z$ can also be safely omitted. Disregarding the second-order derivate $(\partial^2/\partial t^2)P$ of the polarization (in analogy to the microscopic Bloch equations where one implicitly assumes a linear-response function), we finally obtain the following effective wave equation for the counterpropagating $(+,-)$ optical fields in a QD laser:

$$\nabla_T^2 E^\pm\pm 2i\beta\frac{\partial}{\partial z}E^\pm+\frac{\partial^2}{\partial z^2}E^\pm+\frac{2i\omega}{c^2}\frac{\partial}{\partial t}E^\pm-\frac{1}{c^2}\frac{\partial^2}{\partial t^2}E^\pm$$

$$=-\mu_0\omega^2 P^\pm-2i\omega\frac{\partial}{\partial t}P^\pm+F_E q^E(\mathbf{r},t). \qquad (25)$$

The Langevin noise term $F_E q^E(\mathbf{r},t)$ that has been added to Eq. (25) has been derived from quantum Maxwell-Bloch equations [33]. It considers spontaneous light-field fluctuations that depend via $F_E=(\sqrt{2\hbar\omega_0})/(\sqrt{\epsilon_r\epsilon_0})$ on the specific material parameters and on the emission wavelength of the device. $q^E(\mathbf{r},t)$ obeys the correlation relation

$$\langle q^E(\mathbf{r},t)q^E(\mathbf{r}',t')\rangle=\kappa\delta(r-r',t-t'), \qquad (26)$$

where $\kappa=1/(2L)\ln[R_1 R_2]$ corresponds to the damping rate of the resonator. The polarization of the active semiconductor medium

$$P^\pm=V^{-1}\sum_{i,j}d(i,j)p^\pm(i,j) \qquad (27)$$

is the source of the optical fields (V denotes the normalization volume of the crystal).

Our derivation of the QD-MBEs reflects the spirit of describing the (spatiotemporal) dynamics of (spatially inhomogeneous) semiconductor lasers on the basis of Maxwell-Bloch equations [38]. The QD-MBE mesoscopically considers the dynamics of the carrier distributions in the dots and the interlevel dipoles together with the spatiotemporal dynamics of the optical fields [including spontaneous light fields, amplified spontaneous emission (ASE) and induced recombination].

Specific laser configurations of an actual device that is characterized by its geometry, reflectivity of the mirrors, current, injection, etc. are fundamentally included in our description. They enter the theory in the form of boundary conditions for the dynamically varying optical fields and carriers, e.g., the pump term of the QD-MBEs. The laser cavity induces additional counterpropagation and waveguiding effects, which superimpose the carrier-field dynamics. The resulting complex dynamic spatiospectral interactions between the QDs, the optical fields, and the surrounding layers influence the emission properties (e.g., temporal behavior of the optical fields, emission spectra). In the following section we will discuss selective results of numerical simulations that illustrate the interplay of light-field and carrier dynamics in quantum-dot lasers.

III. COUPLED SPATIOTEMPORAL LIGHT-FIELD AND INTERLEVEL/INTRALEVEL CARRIER DYNAMICS IN QUANTUM-DOT LASERS

In the following, we will present selective results of numerical simulations based on QD-MBEs. Specifically, we will consider spontaneous and induced light emission in the active dot medium and analyze the influence of spatial inhomogeneities (in quantum-dot parameters such as dot size, level energies, dipole matrix elements) on the spatiotemporal light-field and carrier dynamics. For specificity, the QDL structure is assumed to consist of three dot layers (InAs/ GaAs [3]) with a dot density of 10^{10} cm^{-2}. The dots are assumed to be of pyramidal shape (with base length 12 nm) with three electron and five hole levels. The length of the laser is 1 mm, its width (of the active zone) 10 μm. At every location within the medium, the QD-SBEs are, via dynamic scattering terms, coupled to a diffusion equation describing the spatial distribution of the carriers in the surrounding layers. The general representation of physical properties and components of a QDL by the QD-MBEs is sketched in Fig. 2: The spatial dependence of the carriers in the wetting layer and the propagating light fields ($E^{\pm}$) are, in the simulation of the spatiotemporal dynamics, considered via a numerical grid with equally spaced grid points in the lateral (x) and propagation (z) direction. The local distribution of QDs is defined by spatial coordinates with respect to this grid. Thereby the spatial distance between the position of each QD and the center of the respective cell (with length Δz and width Δx) is saved in a spatially dependent variable that is used for the collision rates between the QD and wetting layer. Each mesh (size $\Delta x \Delta z$) contains the following information: Number of (effective) QDs in the mesh, N_{QD} (note that a "hole" in the spatially distributed QDs, i.e., $N_{QD}=0$ is also possible), position of the QDs (i.e., their distance from the center of the area ($\Delta x \Delta z$), and the individual material properties of the QDs. The specific laser configuration is defined by the size of the medium and the reflectivities of the facets (R_1, R_2) and enters the theoretical description as boundary conditions for the optical light fields.

A convenient way to visualize the spatiotemporal light dynamics of spontaneous- and induced-emission processes is in the form of temporal and spatial light-field and the carrier distributions. To additionally grasp the complex microscopic carrier-relaxation dynamics we will focus on the dynamics of the level occupations. On route, we will analyze the influence of spatially varying quantum-dot properties (e.g. dot size, level energies, dipole-matrix elements) on the spatiotemporal light-field and carrier dynamics.

A. Spatiotemporal light-field dynamics: Interplay of spontaneous and induced emission

One of the very characteristic properties of a laser is the buildup of coherence in the light field from initial spontaneous emission. In the quantum-dot laser whose active medium is fundamentally characterized by the spatially inhomogeneous ensemble distribution of active quantum-dot sources, one would expect that this transition is determined by this very feature together with the dependence on the (electrical
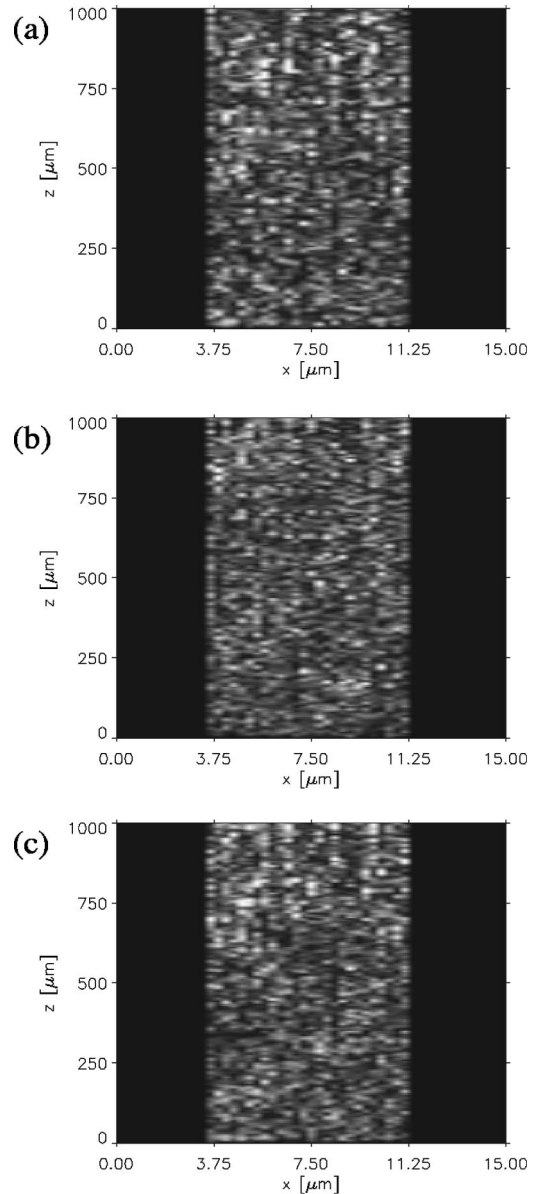

FIG. 3. Dynamics of luminescence patterns of spontaneous emission of an idealized quantum-dot laser with perfect and uniform dot arrangement and identical parameters for dot size, level energies, and dipole-matrix elements. Light shadings indicate high levels of intensity. The time between successive snapshots is 3 psec.

or optical) excitation of the system. For low electrical injection current Fig. 3 shows typical snapshots of the spatial light-field distribution within our model quantum-dot laser structure. The time interval between the snapshots—showing the speckle distribution that is a characteristic of the quantum-dot medium—is 3 psec. In this example we have assumed the very ideal case where the distribution of the dots within the structure is uniform (i.e., the dots are positioned with constant dot-to-dot distance). Furthermore, we have used, for each dot within the structure, an identical set of parameters for dot size, level energies, and dipole-matrix element. The injection of carriers has been chosen such that the occupation of the energy levels of the dots are near transparency. In spite of the "ideal" conditions assumed for the
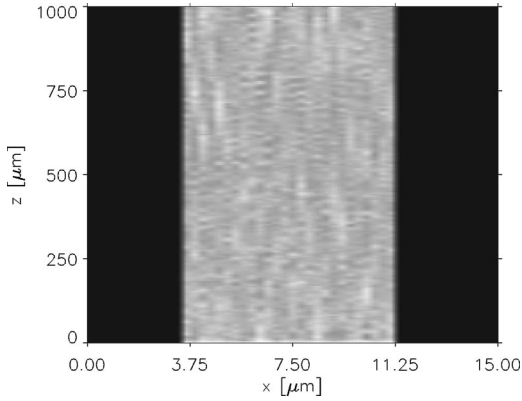
FIG. 4. Snapshot of the spatial electron distribution corresponding to the luminescence pattern of Fig. 1(c).

laser structure, spatial fluctuations in light and carrier distribution arise. They are the result of spontaneous light fluctuations, microscopic carrier-relaxation dynamics, and nonlinear coupling between the light fields and the charge-carrier plasma: The carrier dynamics within each dot is determined by processes such as carrier injection, spectral-hole burning, intradot carrier relaxation via phonon emission and absorption, carrier-carrier and carrier-phonon interaction with the wetting layers, as well as screening. We will later focus on those in more detail. For now we can see that for the light-field dynamics the underlying physical processes consist of both coherent (in the case of, e.g., induced recombination) and incoherent contributions (e.g., spontaneous emission, carrier relaxation). Consequently they vary from dot to dot even when identical dot parameters and ideal uniformity of the dot distribution in the layers are assumed.

The interplay of incoherent and coherent interactions yields a spatially varying number of electrons and holes in the energy levels of the quantum dots. Together, the spontaneous and induced light emitted by a quantum dot then contributes to the forward and backward propagating light fields and is thus transferred to the neighboring dots leading to complex spatiotemporally varying light-matter interactions. The propagating light fields on the other hand, experience a spatially dependent modification via the interaction with the quantum-dot ensemble. In combination with the diffraction of the light field this leads to a spatially varying light-field dynamics [Figs. 3(a)–3(c)]. The nonlinear and inhomogeneous light-matter interaction and the carrier dynamics affect at the same time the spatial charge-carrier density. For the time frame of Fig. 3(c), Fig. 4 shows as an example the distribution of electrons. The spatially varying level occupation and the formation of characteristic optical patterns are a direct consequence of spontaneous light fluctuations and scattering. The microscopic intradot scattering of the carriers within the dots via emission and absorption of phonons, the interaction of the "dot carriers" with the carriers and the phonons of the wetting layer, and the nonlinear coupling to the propagating light fields lead to a spatially varying occupation of the dots and subsequently to complex transverse carrier dynamics. It is important to note that the interplay of light with the carriers results in a spatiotemporally varying occupation although we have assumed the "ideal" case of
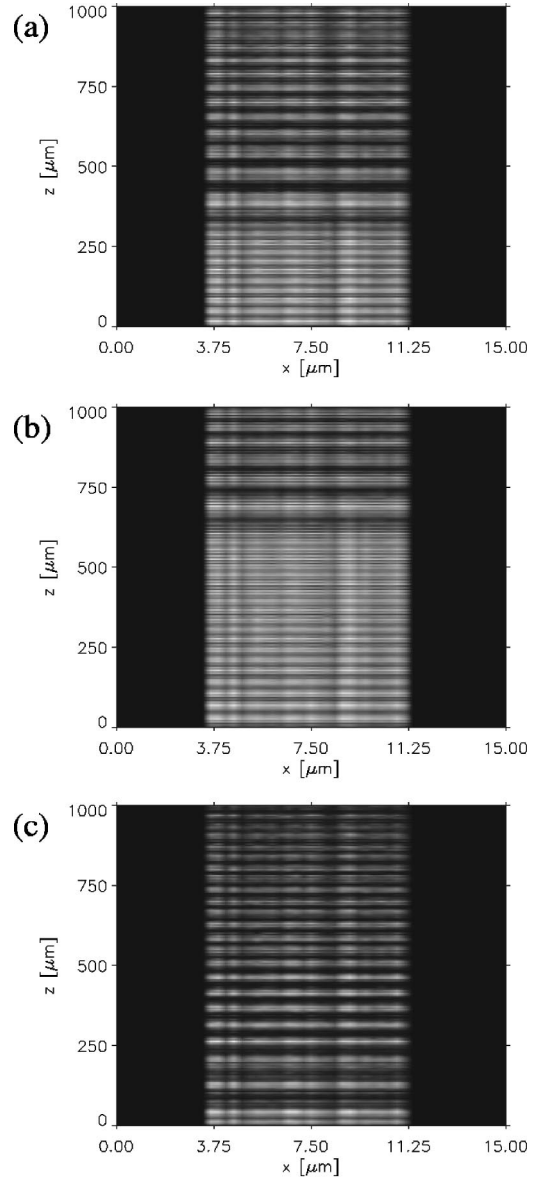

FIG. 5. Spatiotemporal dynamics of stimulated emission in quantum-dot lasers pumped above threshold. The time interval between successive snapshots is 3 psec.

uniform carrier injection and regular matrixlike positioning of quantum dots that each have identical properties (size, level energies, matrix elements).

The spatiotemporal light-field dynamics changes if we increase the excitation level (carrier injection) by rising the respective pump term in the Bloch equations so that the dots are almost completely filled with carriers. In this case the snapshots (again with time steps of 3 psec) of Figs. 5(a)–(c) show the result of a significant inversion: light amplification by induced recombination occurs in addition to the spontaneous-emission processes. The first intensity distribution is taken 100 psec after the initial excitation of the dots. In the longitudinal (z) direction one can observe dynamically varying intensity modulations. These longitudinal structures are typical for the inset of laser oscillations of a device immediately after start-up. They are a measure of the charac-
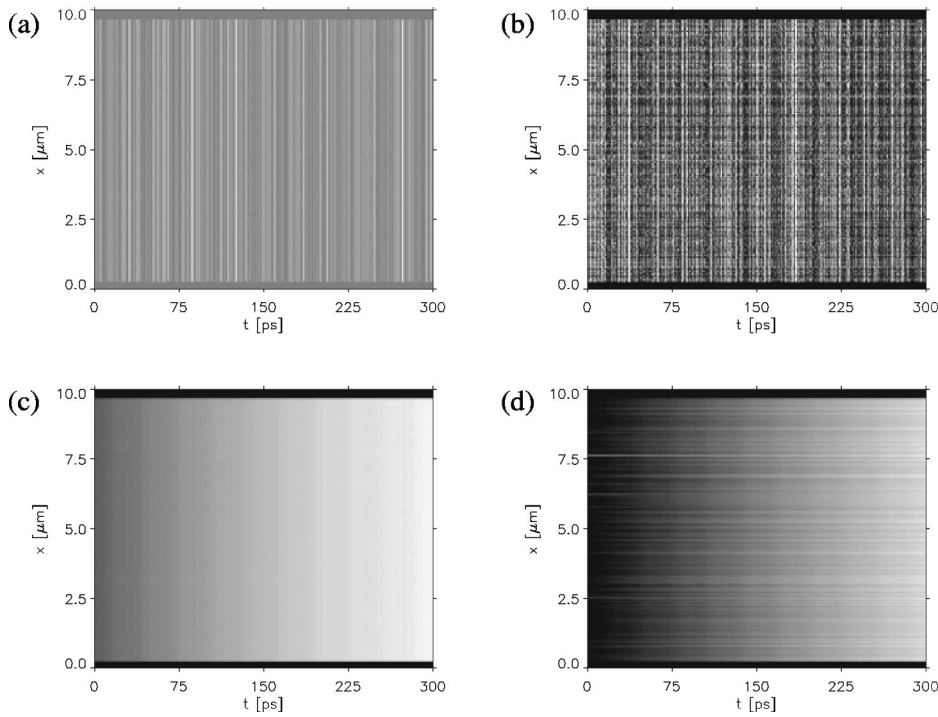
FIG. 6. Dynamics of the optical nearfield (a),(b) and the corresponding carrier density (c),(d) at the output facet of a QDL. (a),(c) for negligible dot-to-dot fluctuations, (b),(d) quantum-dot ensemble with Gaussian fluctuations (with a variance of 12%) in size and location.

teristic internal coherence length scales that typically lie in the micron regime. In time, the structures lead to intensity spiking and relaxation oscillations in the light emission. In lateral direction, i.e., parallel to the output facet, the intensity is rather uniform when compared to Fig. 3. This uniformity originates from induced emission processes, which now play a major role in the overall behavior of the device: The initial filling of the dots establishes a carrier inversion and thus a high gain. Due to the increased influence of induced-emission processes, a spatiotemporal coherence builds up, which is via the propagating light fields transferred in both time and spatial dimensions. The coupling of the carriers in the dots with the propagating light fields in combination with the high gain characterizing the dot medium may then lead to a narrow-band stable laser output.

B. Spatial fluctuations

Contrary to the ideal situation assumed so far, slight dot-to-dot variations in size, energy levels, and material parameters exist in real quantum-dot laser systems. In addition, the dots are not equally positioned on a grid within the layers. The respective variance in quantum-dot parameters and dot-to-dot distance depends on the material system and the epitaxial growth process of the particular quantum-dot system. The most relevant inhomogeneities are, e.g., a variance of QD size, energy levels, dipole-matrix elements, and nonuniformities in the distribution of quantum dots in the layer.

To elucidate the influence of spatial fluctuations, we will contrast the temporal behavior of the near-field intensity and the carrier density at the output facet of an almost ideal quantum-dot laser (with uniformly distributed, almost identical dots) with a quantum-dot laser characterized by strong spatial dot-to-dot fluctuations (of 12%) in the parameters. Figure 6 displays in a time window of 300 psec (starting

approximately 200 psec after turning on the device) the dynamics of the optical nearfield (a),(b) and the carrier density (c),(d) at the output facet of the laser. In Figs. 6(a) and 6(c) only a negligible deviation of the QD parameters from their average values has been chosen (1% variance) while in case of Figs. 6(b) and 6(d) the variance of the parameter values of the spatially distributed QDs (i.e., their size, dipole-matrix elements, energy levels) is Gaussian with a variance of 12%. In both situations (low and high fluctuations) the near-field intensity [Figs. 6(a) and 6(b)] shows slight modulations on a picosecond time scale. They originate from the dynamic interactions between the light fields and the QD carriers ranging from the femtosecond time scale (in the case of microscopic carrier scattering) up to the picosecond and nanosecond time scales (reflecting the resonator round trip time of the propagating light fields and the slow buildup and decay of the spatial carrier density). From the simulations we can see that the diffraction of the light fields and the spatially dependent interaction of light with the carriers in the dots and in the wetting layer lead to the formation of characteristic optical patterns. The time scales of the carrier dynamics thereby are via the propagation of the light fields transformed into characteristic interaction lengths like the coherence length. In combination with the diffraction of the light fields this leads to transverse modulations in Fig. 6 that typically lie in the micron regime.

The light-field dynamics is determined on the one hand by the induced and spontaneous recombination processes and on the other hand indirectly by carrier scattering via carrier-carrier and carrier-phonon interactions. The mutual influence of light and matter is particularly strong during the start-up regime of the laser and leads to characteristic oscillations in the time domain. In case of a laser with a high spatial variance of the QD parameters, the spatial dependence of the near field is strongly affected: The spatial fluctuations in size

and energy levels of the dots are via the term $i\bar{\omega}+\gamma_p$ of the QD Bloch equations [see Eq. (1)] transferred to spatiospectral changes in the interlevel polarization. Changes in the dipole-matrix element $d(i,j)$ induce via $(i/\hbar)(n^e+n^h)E^{\pm}$ respective changes in the interlevel polarization. This leads—via the spatial polarization of the wave equation (25)—to dynamic changes in both, amplitude and phase of the propagating light field and thus to the formation of dynamic characteristic optical patters. The spatial dynamics and relaxation of the carrier density typically occurs on longer time scales of a few hundred picoseconds. Thus in the time window of Figs. 6(c) and 6(d) the increase in carrier density is part of a relaxation oscillation. In addition to the uniform increase in the carrier density, Fig. 6(d) shows a characteristic filament structure. They originate from the mesoscopic coupling of the charge-carrier plasma and the light-field dynamics. The dynamic changes in the carrier system depend, via the generation rate of the Bloch equations [see Eqs. (1)], on the light fields that are spatiotemporally modified by the spatially varying dot parameters. In addition, carrier-relaxation processes, via phonon emission or absorption and via interaction with carriers and phonons of the wetting layers, depend on the energy differences of the levels involved and thus are also directly affected by the spatially varying dot parameters. We note that although we have in our example chosen the fluctuations of the respective parameters to be the same in each dot, the variance of the individual parameters can, in principle, be chosen independently.

C. Ultrashort-pulse propagation in a quantum-dot waveguide

A typical means of probing the internal dynamics of a quantum-dot laser is to inject an optical pulse into the laser and analyze the ultrafast dynamics of the output signal. For this configuration thus one additionally has to consider a light pulse propagating in a laser waveguide (width of the structure 10 μm, length 1 mm) filled with an inverted quantum-dot ensemble. The snapshots displayed in Fig. 7 show the intensity (a)–(c) and the carrier density (d)–(f) within the active area of a QD laser during the propagation of an ultrashort light pulse whose frequency corresponds to the transition energy of the QDs. The injection current density has been chosen such that the population of the dots within the layers of the QD waveguide are significantly above the transparency. For the dot-to-dot fluctuation a variance of 5% has been assumed. The time between successive plots is 3 psec. Figs. 7(a) and 7(d) represent the spatial distributions of the intensity (a) and the carrier density (d) immediately after optical injection. It is important to note that initially the lateral spatial shape of the injected light field is Gaussian shaped with a width full width at half maximum of 6 μm and the temporal profile of the pulse is chosen Gaussian as well with a full width at half maximum of 500 fsec. Immediately after injection the light pulse starts to interact with the ensemble of populated QDs. During its propagation through the laser the pulse locally reduces the population within the dots established by the injection current by induced recombination. With continuing propagation the light pulse is significantly amplified Fig. 7(b). Due to the nonlin-
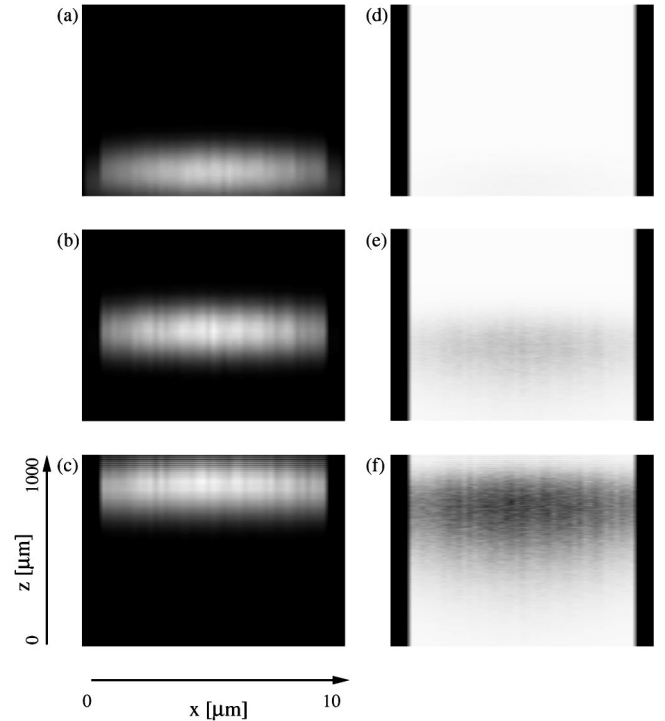

FIG. 7. Propagation of a femtosecond pulse (full width at half maximum of 500 fsec) tuned to resonance of an inverted quantum-dot ensemble. (a)–(c) Snapshots of the light field and (d)–(f) corresponding snapshots of the carrier density. The time between successive snapshots is 3 psec.

ear light-matter interaction between the pulse and the spatially distributed dots, a complex spatiotemporal behavior arises. It is directly reflected in the dynamic spatial structures in both intensity and carrier density. The pulse is laterally structured and temporally distorted via the interaction with the dots [Figs. 7(b) and 7(c)]. At the same time, spatial-hole-burning effects can be observed in the carrier distribution of Figs. 7(e) and 7(f). The partial refilling of the dots—determined by carrier injection, carrier capture, and thermalization via carrier relaxation—defines a finite "response time" of the QD medium. As a consequence, the spatial extension of the hole burnt by the light pulse [Fig. 7(f)] significantly exceeds the spatial area covered by the optical pulse [Fig. 7(e)]. Thus, a light pulse propagating in a QD waveguide is strongly modified by the nonlinear interaction with the QD system. The amount of spatial and temporal distortions the light pulse experiences thereby strongly depends on both spatial effects (such as dot density, uniformity of the dot distribution, spatial fluctuations) and microscopic "spectral" effects (determined by the characteristic relaxation times and microscopic dot properties). The spatial effects displayed in Fig. 7 are thus—via the coupling between the wave equation and QD-Bloch equations—the result of microscopic physical effects. In order to analyze these dynamics we will in the following focus on the population changes induced by a light pulse.

D. Interlevel and intralevel carrier dynamics of the quantum-dot ensemble

While the optical output signal carries information on the carrier dynamics of the quantum-dot ensemble, it does not
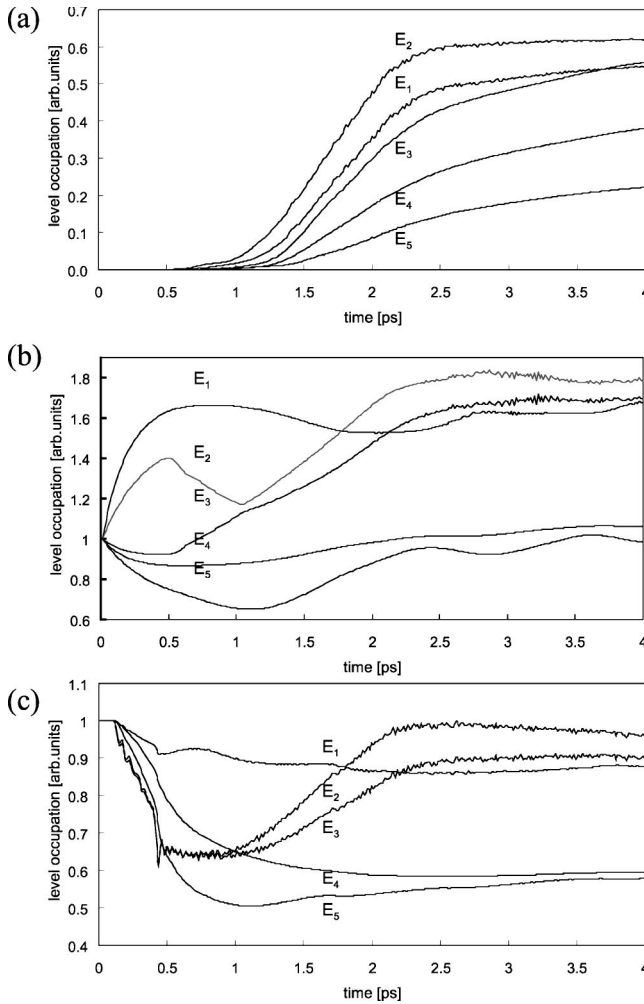
FIG. 8. Calculated hole-level occupation during the propagation of a light pulse: (a) absorption, (b) transparency, (c) amplification.

directly reveal the carrier dynamics within each energy level. In our QD-MBE the interlevel and intralevel dynamics are automatically represented and calculated. The level dynamics allows a visualization of the microscopic interactions occurring within the dots. As an example, we will concentrate on results calculated for the hole-level occupation during the propagation of a light pulse (500 fsec). The respective electron-level occupations show a qualitatively similar behavior. We will focus on three physically different situations: absorbing, transparent, and amplifying QD media. Figure 8(a) shows the situation where the energy levels are almost empty at the start of the calculation. In this case the pulse leads to an optical excitation of the carrier system. If on the other hand the dots are initially significantly filled [Fig. 8(c)], an effect similar to the well-known spectral hole burning occurs: Depending on the dipole-matrix elements for the individual states and depending on the frequency detuning of the pulse with respect to the frequency of the respective electron and hole states, a reduction of the individual level occupation and a partial refilling via carrier injection and microscopic scattering processes occurs. The microscopic scattering processes involved in this "level burning" are determined by emission and absorption of phonons, mul-

tiphonon interactions, and the interaction with the carriers and phonons of the wetting layer.

The magnitude of the various "channels" for relaxation mechanisms thereby depend on the QD energy levels, on the energy difference of the surrounding layers, and on the coupling of a dot to its next neighbors. This dot-to-medium and dot-to-dot interactions thereby are determined by the dot density and the light propagation that mesoscopically couples the QDs. It is consequently both specific material properties and dynamic light-matter interactions that decide whether the dots are isolated from their environment or behave like a thermalized ensemble. In passing we may remark that it is a decisive advantage of the mesoscopic spatial resolving that every intermediate state of the dots is allowed without restriction to the limiting cases of full isolated dots or a completely thermalized set of dots.

The physical situation is particularly interesting if the dot medium is near transparency [Fig. 8(b)]. Due to the individual matrix elements the occupation of the various levels may rise or be reduced even though the sum of all contributions stays more or less at a constant value. In particular, the dynamic changes in the level occupation and the dynamic saturation of individual levels may lead to the situation that the laser first saturates to a specific level and then changes from one interlevel transition to another one.

E. Luminescence of optically excited quantum-dot media

In Sec. III C we have considered the propagation of a resonant light pulse in an inverted quantum-dot medium, i.e., an electrically pumped QDL. While this certainly represents the preferred mode of operation of quantum-dot lasers in most applications, in many current experimental setups, however, one investigates luminescence of optically excited quantum-dot media by an (ultra) short optical-pump pulse. In the quantum-dot laser this corresponds to an approximately δ-shaped excitation of carriers into one or more high-energetic carrier reservoirs either in the dots themselves (direct optical pumping) or by carrier capture from the optically pumped wetting layer (indirect pumping). Since the dynamic interplay between the dots and the wetting layer is determined by a large variety of relaxation processes involving the dot carriers and the carriers in the wetting layer, the excitation of the dots via the wetting layer represents a particularly interesting case. In the following we will thus focus on the case of an ensemble of (initially empty) dots that is dynamically filled from the wetting layer (the high-energetic carrier-reservoir). The dynamic coupling between the dot carriers and the carriers of the wetting layer is determined by the density of quantum dots, the individual dot properties, and the epitaxial growth process. These factors contribute simultaneously and lead to a characteristic response of the quantum-dot system. Thus the resulting luminescence is influenced by and directly reflects the multitude of physical quantities that are involved in the characteristic excitation and relaxation processes. These are characteristic (material) properties like the optical matrix elements for the various (intradot and dot-wetting layer) carrier and carrier-phonon interactions, the transition-matrix elements of the dot levels
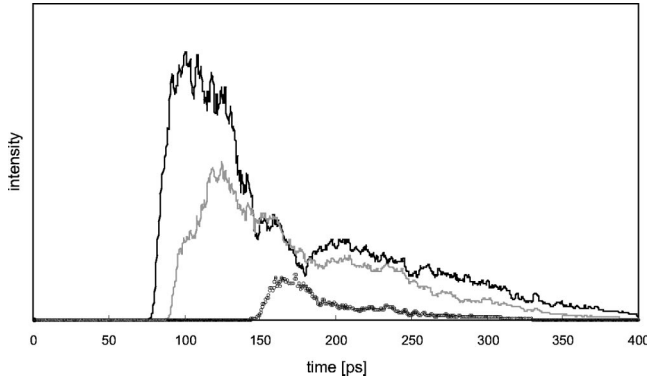
FIG. 9. Dependence of the QD luminescence on excitation level. Solid, gray, and dotted lines correspond to competely, half, and significantly less than half filled wetting-layer states, respectively.
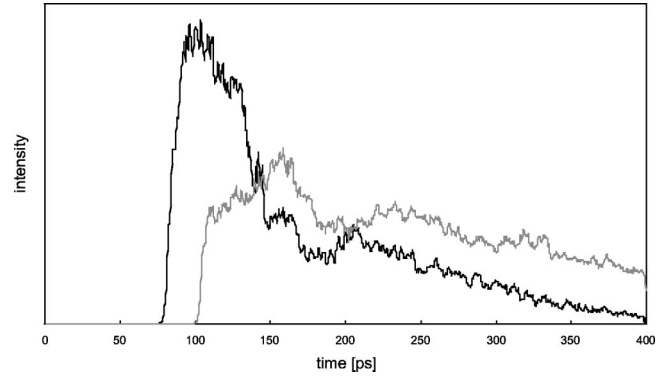

FIG. 10. Dependence of the QD luminescence on coupling strength. High coupling strength (black) provides a fast filling and efficient refilling of the dots that are partially depleted via induced-emission processes. Weak coupling (gray) leads to a gradual depletion of the carrier reservoir.

involved, the energies of the dot levels and the wetting-layer states, the dot density, and the spatial dot distribution. Since a detailed analysis and variation of all these parameters (some of which even are presently not known in detail) involves extensive simulations we will in the following restrict ourselves to the investigation of the influence of the filling degree, the coupling strength, and the energy levels. Thereby we implicitly assume the remaining parameters to be (spatially dependent) constants.

Figures 9, 10, and 11 show the characteristic luminescence, i.e., the laterally averaged intensity at the output facet of an optically pumped QDL structure. The degree of initial filling of the high-energy reservoir and the coupling strength between the dots and their environment determines the time constants for carrier capture into the dots and the degree of dot filling. In combination this may lead to very different characteristic emission behavior discussed below.

1. Influence of excitation strength

The three curves displayed in Fig. 9 show the dependence of the luminescence on the filling degree of the carrier reservoir. The solid, gray, and dotted lines visualize the situation where all, half, and significantly less than half of the available wetting-layer states are filled with carriers, respectively. For a moderate initial excitation the loading of the QDs with carriers is comparatively slow, leading to a delayed onset of light emission. An increase in the initial carrier filling of the reservoir provides a higher inversion in the dots resulting in intense light emission. The variation of the reservoir not only determines the instant and intensity of the light emission, it also affects the shape of the curve: For high excitation a selective saturation of individual transitions may occur. As a consquence, a second transition can be involved leading to mode beating, temporal modulations, or a second peak in the emission curve.

2. Influence of coupling strength

In order to analyze the influence of the coupling strength we have calculated the intensity and level occupation in the dots with dependence on the fraction of wetting-layer states to which the dots couple (normalized to a unit cell

$\Delta z \times \Delta x$). In a given laser structure this value is determined by the dot density and by the potential step between the dots and their environment determined by the size and shape of the dots as well as the particular material systems and epitaxial growth processes. The resulting dynamic behavior of the emitted intensity is depicted in Fig. 10. First, a high coupling strength provides a faster filling of the (initially) empty dots. As a consequence, the dot occupation reaches the characteristic threshold value that is apparent in Fig. 10 at an earlier time step. Second, it enables an efficient refilling of the dots that are partially depleted via induced-emission processes. In combination this leads to an intense peak in the emission curve (black). A weak coupling on the other hand (gray) leads to a slow depletion of the carrier reservoir. As a result it delays the onset of light emission and ''stretches'' the shape of the emission curve in time.

3. Influence of quantum-dot size and growth: Variation of energy levels

A variation in size and epitaxial growth of a quantum dot has a direct consequence for its energy levels. These variations in eigenenergies directly enter the QD-Bloch equations. In the following we will consider two channels of transitions with the highest transition-matrix elements for two different cases: (1) a QD system with close transition energies (i.e., separated by less than the LO phonon energy) and (2) a QD system where the carrier levels belonging to the two most dominant transitions differ by an energy much higher than the LO phonon energy. For these two examples Fig. 11 shows the temporal behavior of the (electron) level occupations [Fig. 11(a)] and the resulting emission curve [Fig. 11(b)] after the initial excitation of the QDs. The black lines in Fig. 11(a) pertain to the QDL where the transitions with the highest matrix elements are separated by more than the LO phonon energy. The gray curves correspond to the situation where the respective transition energies are very close to each other. For the example with higher level separation the carriers populating the two QD levels are in main parts decoupled: the carrier recombination mostly restricts to one level (belonging to the transition with the highest dipole-
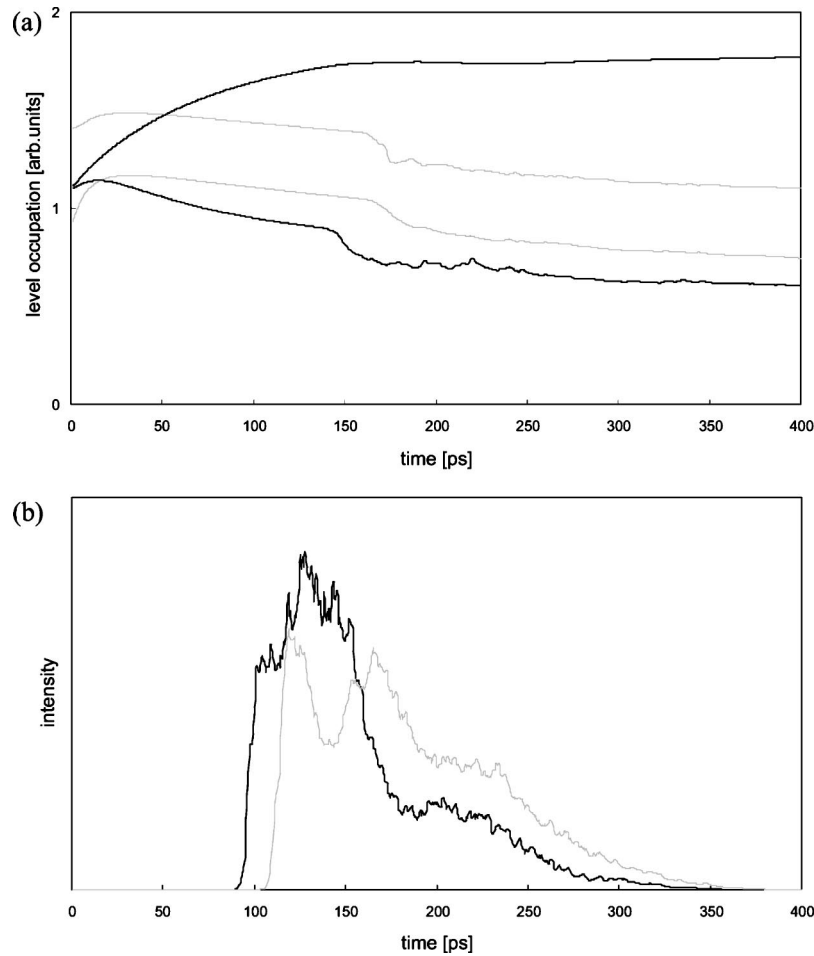
FIG. 11. Dependence of (a) level occupation and (b) the QD luminescence on transition energies. The black lines pertain to a QDL, with the highest matrix elements separated by more than the LO phonon-energy. The gray curves illustrate the case where the respective transition energies are very close to each other. The respective emission properties represented by the solid curve in (b) show one intense peak belonging to the main transition. The dashed curves visualize the carrier occupation for the dot system with close transition energies.

matrix element) whereas the second level absorbs carriers from the reservoir. The respective emission properties represented by the black curve in Fig. 11(b) shows one intense peak belonging to the main transition. For the same excitation conditions, the dashed curves visualize the carrier occupation for the dot system with close transition energies. In this situation the two main carrier levels interact and "interfere" via dynamic carrier and phonon scattering. The resulting emisssion curve (gray) shows two maxima. The specific shape of the temporal emission characteristics thus is a direct consequence of the dynamic interplay of competing transitions and spectral modes.

IV. CONCLUSION

In conclusion, we have set up a mesoscopic theory on the basis of a Maxwell-Bloch description. The resulting QD-MBEs consist of coupled spatiotemporally resolved wave equations and QD-Bloch equations for the electron and hole levels within each quantum dot of a quantum-dot ensemble inside a quantum-dot laser.

We have presented results of our numerical simulations that aim to mesoscopically represent realistic QD laser structures. The simulations include, in particular, microscopic QD properties, spatially dependent QD parameters and fluctuations, spatially inhomogeneous light propagation, and dynamic scattering. The carrier-scattering processes are considered on a mesoscopic level and include both the intradot relaxation and the interactions between the QD carriers and the surrounding layers. The specific laser configuration of a model device is considered via the macroscopic boundary conditions and constraints. The QD-MBEs allow the calculation and visualization of spatial distributions of the light-field intensity and carriers. Furthermore, the calculation of level occupations provides a detailed analysis of the various relaxation processes. For a specific set of parameters, the quantum dot Maxwell-Bloch equations will allow a microscopically founded interpretation of the QD properties obtained from experimental investigations. Our mesoscopic theory may thus establish a basis for linking the microscopic analysis of QD material properties with the quantum electronics of modern quantum-dot laser systems.

[1] G. Cipriani, M. Rosa-Clot, and S. Taddei, Phys. Rev. B **61**, 7536 (2000).

[2] T. Inoshita and H. Sakaki, Phys. Rev. B **56**, R4355 (1997).

[3] O. Stier, M. Grundmann, and D. Bimberg, Phys. Rev. B **59**, 5688 (1999).

[4] W. Yang, H. Lee, T. Johnson, P. Sercel, and A. Normann, Phys. Rev. B **61**, 2784 (2000).

[5] A.J. Williamson and A. Zunger, Phys. Rev. B **59**, 15 819 (1999).

[6] A. Williamson and A. Zunger, Phys. Rev. B **61**, 1978 (2000).

[7] E. Dekel, D. Gershoni, E. Ehrenfreund, J. Garcia, and P. Petroff, Phys. Rev. B **61**, 11 009 (2000).

[8] R. Rinaldi, S. Antonaci, M.D. Vittorio, R. Cingolani, U. Hohenester, E. Molinari, H. Lipsanen, and J. Tulkki, Phys. Rev. B **62**, 1592 (2000).

[9] G. Narvaez and P. Hawrylak, Phys. Rev. B **61**, 13 753 (2000).

[10] M.-C. Cha and S.-R.E. Yang, Phys. Rev. B **61**, 1720 (2000).

[11] N. Bruce and P. Maksym, Phys. Rev. B **61**, 4718 (2000).

[12] R.J. Warburton, B.T. Miller, C.S. Drr, C. Bdefeld, K. Karrai, J.P. Kotthaus, G. Medeiros-Ribeiro, P.M. Petroff, and S. Huant, Phys. Rev. B **58**, 16 221 (1998).

[13] X.-Q. Li and Y. Arakawa, Phys. Rev. B **56**, 10 423 (1997).

[14] U. Bockelmann, Phys. Rev. B **48**, 17 637 (1993).

[15] T. Stauber, R. Zimmermann, and H. Castella, Phys. Rev. B **62**, 7336 (2000).

[16] M. Braskén, M. Lindberg, D. Sundholm, and J. Olsen, Phys. Rev. B **61**, 7652 (2000).

[17] X.-Q. Li, H. Nakayama, and Y. Arakawa, Phys. Rev. B **59**, 5069 (1999).

[18] R. Ferreira and G. Bastard, Appl. Phys. Lett. **74**, 2818 (1999).

[19] J.L. Pan and P.L. Hagelstein, Phys. Rev. B **49**, 2554 (1994).

[20] A.V. Uskov, K. Nishi, and R. Lang, Appl. Phys. Lett. **74**, 3081 (1999).

[21] K. Oshiro, K. Akai, and M. Matsuura, Phys. Rev. B **59**, 10 850 (1999).

[22] U. Hohenester, F. Rossi, and E. Molinari, Solid State Commun. **111**, 187 (1999).

[23] H. Tsuchiya and T. Miyoshi, J. Appl. Phys. **83**, 2574 (1998).

[24] H. Tsuchiya and T. Miyoshi, Solid-State Electron. **42**, 1443 (1998).

[25] H. Jiang and J. Singh, J. Appl. Phys. **85**, 7438 (1999).

[26] D.G. Deppe, D.L. Huffaker, S. Csutak, Z. Zou, G. Park, and O.B. Shchekin, IEEE J. Quantum Electron. **35**, 1238 (1999).

[27] S. Grosse, J.H.H. Sandmann, G. von Plessen, J. Feldmann, H. Lipsanen, M. Sopanen, J. Tulkki, and J. Ahopello, Phys. Rev. B **55**, 4473 (1997).

[28] M. Sugawara, K. Mukai, Y. Nakata, H. Ishikawa, and A. Sakamoto, Phys. Rev. B **61**, 7595 (2000).

[29] M. Grundmann, R. Heitz, D. Bimberg, J.H. Sandmann, and J. Feldmann, Phys. Status Solidi B **203**, 121 (1997).

[30] *Quantum Dot Lasers*, edited by M.G.D. Bimberg and N.N. Ledentsov (Wiley, Chichester, England, 1998).

[31] B. Hanewinkel, A. Knorr, P. Thomas, and S.W. Koch, Phys. Rev. B **55**, 13 715 (1997).

[32] O. Mauritz, G. Goldoni, F. Rossi, and E. Molinari, Phys. Rev. Lett. **82**, 847 (1999).

[33] H.F. Hofmann and O. Hess, Phys. Rev. A **59**, 2342 (1999).

[34] P.G. Bolcatto and C.R. Proetto, Phys. Rev. B **59**, 12 487 (1999).

[35] J. Schilp, T. Kuhn, and G. Mahler, Phys. Rev. B **50**, 5435 (1994).

[36] A.V. Uskov, J. McInnerney, F. Adler, H. Schweizer, and M.H. Pilkuhn, Appl. Phys. Lett. **72**, 58 (1998).

[37] *Wave Mechanics Applied to Semiconductor Heterostructures*, edited by G. Bastard (Halsted, New York, 1988).

[38] O. Hess and T. Kuhn, Phys. Rev. A **54**, 3347 (1996).